Chemistry and Technology of Samarium Monosulfide

O.V. Andreev[1*], V.V. Ivanov[2], A.V. Gorshkov[2], P.V. Miodushevskiy[3], and P.O. Andreev[1]

[1]Tyumen State University, Volodarskogo str. 6, Tyumen, 625003 Russia
[2]Closed joint-stock company "TECHNOCOMPLEKT" , Shkolnaya str. 10a, Dubna, Moscow oblast, 141981 Russia
[3]Dubna International University, Universtitetskaya str. 19, Dubna, 141980 Russia

Article info

Abstract

Samarium monosulfide SmS (Fm3m, a = 5.967 Å, ΔE = 0.23 V, n = 10^{20} cm^{-1}, σ = 500 Ω^{-1} cm^{-1}, α = 350 µB/K) is a thermoelectric material (Z>1) and, at the same time, a pressure-sensitive material (K≥40–50). Samarium monosulfide is a daltonide phase with a solid solution whose extent is mostly in the range of cationic vacancies: Sm_{1+x} $S_{1-x}\square_{2x}$ (x = 0–0.035; 1750 K). The congruent melting temperature of SmS is 2475 K. In the Sm–S system, Sm_3S_4 crystallizes from melt without change in composition. Samarium monosulfide thermally dissociates to Sm_3S_4 and Sm. Large-scale SmS lots are produced from samarium and sulfur. Synthesis is carried out in sealed-off silica glass ampoules at 500–1350 K followed by heat treatment in tantalum crucibles at 1500–2400 K. The reaction of metal samarium with sulfur results in the formation of sulfide phases that coat the samarium surface in the following order: SmS, Sm_3S_4, Sm_2S_3, and SmS_2. Subsequent annealing at 1500–1800 K provides SmS yields up to 96–97 mol %. Equilibrium minor phases for SmS are Sm_3S_4, Sm_2O_2S, and Sm. X-ray amorphous SmS was prepared by reacting organic samarium compounds with sulfur or H_2S. The samarium (+2) oxidation state determines the chemical specifics of SmS. 90–120 µm SmS powders are thermally hydrolyzed starting at 600 K with H_2 evolution and oxidize starting at 520 K to yield Sm_3S_4 and then Sm_2O_2S phases. A 90–120 µm SmS fraction for film deposition by flash evaporation is prepared by milling annealed SmS samples. Tablets 75 mm in diameter for use in magnetron sputtering are pressed from a <60-µm fraction.

1.Introduction

Samarium monosulfide is an advanced material that has a unique set of physical and chemical properties [1–3].

In the compound $Sm^{2+}S^{2-}$ (Sm $4f^65d^06s^2$), the 6s electrons of samarium atoms are involved in bonding with sulfur anions. The 4f level lies within the bandgap. Samarium monosulfide is an n-type conductor with charge carrier concentrations on the order of 1020 cm^{-3} [4, 5]. The electrical conductivity of SmS is 500 $\Omega^{-1}\cdot cm^{-1}$ and changes considerably over the extent of $Sm_{1+x}S_{1-x}\square_{2x}$ solid solution ($\square$ – stands for an anionic vacancy; x = 0-0.035). SmS is distinguished from the other $Ln^{2+}S$ compounds by the least energy difference between the 4f level and the bottom of the bandgap, equal to 0.23 eV [4, 6]. When a SmS sample is exposed to linear or volumetric pressure, its electrical conductivity increases linearly as a function of the applied pressure. The linear trend is observed at temperatures of up to 345 K, in some cases up to 470 K. SmS samples are superior to metal pressure sensors in their pressure sensitivity coefficients K (for SmS, K ranges from 40–50 in polycrystalline films to ≤260 in single crystals, against K = 2–4 for metals) [2, 7, 8].

In some technological and performance aspects, SmS pressure sensors are also advantageous over sensors based on compound semiconductors (K = 50–100) and single-crystal silicon (K = 100–135) [9–11].

Samarium monosulfide is an efficient high-temperature thermoelectric material with the figure of merit Z>1 [12]. In thin films, SmS manifests a thermovoltaic effect; a voltage of about 1.1 V appears on a thin-film sandwich structure in a temperature range of 360–428 K [13, 14]. Heat absorption was observed in SmS single crystals in the temperature

---

* Corresponding author. E-mail: o.v.andreev@utmn.ru

range of the thermovoltaic effect. Heat absorption was shown to arise from the collective injection of electrons from donor levels into the conduction band [15, 16].

There are a lot of publications concerned with samarium monosulfide, but there have been no surveys on its chemistry and technology.
This article summarizes the results of our studies and other published data on the chemistry and technology of samarium monosulfide.

2. Experimental

Samarium sulfides were prepared from distilled samarium metal (Sm^{-1} type) and sulfur (a special grade chemical). Weighted samples of the elements were placed in silica glass ampules, which were then degassed and sealed off. The ampoules with samples inside were treated in a muffle at 500–1500 K. As-prepared batches were stirred, compacted, and then heat-treated in tantalum crucibles under an argon atmosphere on a UIN-16-200 induction setup [3, 25, 30]. The compound Sm_2S_3 was prepared from Sm_2O_3 (D type) in an $H_2S + CS_2$ flow at 1200–1300 K [25].

Surface images of particles were obtained using a JSM-6510LV (JEOL) scanning electron microscope. The operation conditions were an accelerating voltage of 20–30 kV and SpotSize of 30–50. Microstructural analysis was carried out with an AxioVert.A1MAT microscope using the AxioVision SE64 program package at a resolution of 0.5 μm [3].

Differential scanning calorimetry was performed on a Setsys Evolution 1750 (TGA–DSC 1600) setup using the SETSOFT 2000 program package, Pt/PtRh (10%) thermocouple in a temperature range of 300–1870 K. Overlapping peaks were resolved by the Thermogram Analyser program [3, 43]. The atmosphere was argon (99.999 wt.% pure). Simultaneous thermal analysis was carried out on an STA 449 F3 Jupiter analyzer in the temperature range 400–2000 K using a tungsten–rhenium thermocouple. A high-purity (99.9999999 wt.%) helium flow was created in the system during the experiment. Peak areas were determined by the Proteus 6 2012 program. Visual polythermal analysis was performed on a VPTA-1M setup with a precision of within 1% of the measured value [43].

X-ray powder diffraction patterns were recorded on a PANalytical X'Pert PRO diffractometer (CuK_α radiation, Ni filter, PIXcel detector) over the 2θ range from 10° to 100° [43].

The phase composition of surface layers (to

depths of 0.5–1.0 nm) was studied by Auger spectroscopy (VG ESCALAB 210) [31].

Films were prepared on a flash evaporation setup [43] or a Nanofab-100 magnetron sputtering experimental aggregate [17].

3 Results and Discussion

The Sm–S system forms samarium sulfides represented by rational formulas with integer indices, namely SmS, Sm_3S_4, α-Sm_2S_3, and γ-Sm_2S_3 [18], as well as compounds represented by irrational formulas, namely $SmS_{1.86}$, $SmS_{1.89}$, and $SmS_{1.90}$ [19].

The samarium sulfides are mainly categorized into sulfides proper and polysulfides. In full-valence sulfides SmS, Sm_3S_4 ($Sm^{2+}Sm^{3+}_2S_4$), α-Sm_2S_3, and γ-Sm_2S_3, there exist only sulfide sulfur anions S^{2-} in the structure. In polysulfide compounds, there are $(S–S)^{2-}$ groups [18, 19].

Cubic polysulfide SmS_{2-x} (x = 0–0.18; 64–66.6 at. % S) is formed by the direct reaction of samarium with sulfur inside a silica glass ampoule (Table 1). Thus-prepared samples are not equilibrated. Vasileva [19] measured vapor pressure above solid polysulfides and discovered that three compounds of constant composition, namely $SmS_{1.86}$ (65.03 at. % S), $SmS_{1.89}$ (65.4 at. % S), and $SmS_{1.90}$ (65.52 at. % S), are formed in the range of 64.5–66.6 at. % S. We have not found structure data for these compounds.

The thermal stability of samarium sulfides and polysulfides is determined by the type of sulfur anion involved.

The cubic unit cell of SmS is a basic one and can be transformed to unit cells of other samarium sulfides (Fig. 1, Table 1) [20].
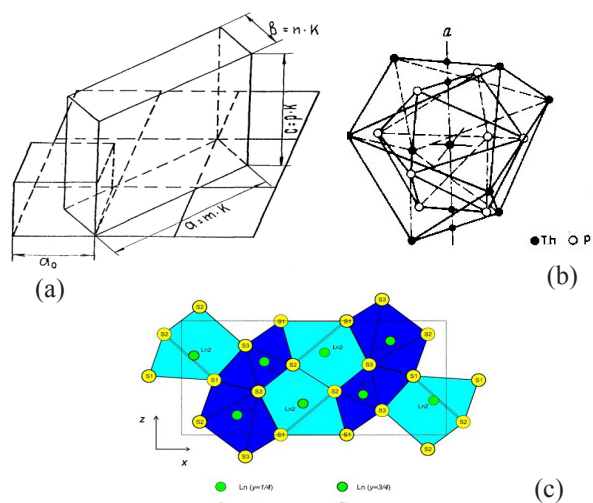

Fig. 1. Scheme of transition from (a) the cubic unit cell to (b) Th_3P_4 type and (c) α-Ln_2S_3 type unit cells of rare-earth sulfides. m, n, and p are integers [18, 20].

Table 1
Crystal data for samarium sulfides [3, 4, 18]

Sulphide	Color	Crystal structure	Space group	Structural type	Period of cell, Å			Density, g/cm³	
					a	b	c	Picnometric	X-rays
SmS	Black	Cubic	Fm3m	NaCl	5.967			5.64	5.67
Sm₃S₄	Black	Cubic	I43d	Th₃P₄	8.556			6.11	6.14
α-Sm₂S₃	Cherry	Rhombic	Pnma	α-La₂S₃	7.382	3.974	15.372	5.59	6.09
γ-Sm₂S₃	Yellow	Cubic	I43d	Th₃P₄	8.448			5.77	5.83
SmS₂₋ₓ	Black	Cubic		LaS₂	7.965			5.56	5.66

In the γ-Sm_2S_3 cubic structure, every ninth position in the cationic sublattice is vacant; the crystal formula is $[Sm_8\square]S_{12}$. When the vacancies are completely occupied, the composition is Sm_3S_4 [3, 18].

In the solid solution $[(Sm^{3+})_{(8-2x)/3}Sm_x^{2+}\square_{(1-x)/3}]S_4$ ($\square$ – stands for a cationic vacancy; $x = 0$–1), there exists a general sulfur anionic sublattice. The cationic sublattice contains randomly distributed di- and trivalent samarium ions and cationic vacancies. In the range of compositions from γ-$SmS_{1.4}$ to γ-$SmS_{1.5}$, vacancy ordering can occur [21, 22].

The Sm–S phase diagram shown in Fig. 2 was constructed using data borrowed from [3, 4, 22] and our own data.

Within the range of compositions between 50 and 60 at. % S, congruently melting compounds are formed in the Sm–S system: SmS ($T_m = 2475$ K), Sm_3S_4 ($T_m = 2355$ K), and Sm_2S_3 ($T_m = 1990$ K). The congruent melting temperatures of these compounds were determined by VPTA accurate to ± (25–50) K. At temperatures above 1470 K there exists a Th_3P_4-type solid solution between Sm_3S_4

and γ-Sm_2S_3 phases (Fig. 2) [3, 22].

Samarium sulfides dissociate as temperature rises. The thermal dissociation of SmS starts long before the phase melts. In samples annealed at 1800–1850 K, X-ray powder diffraction and microstructure examination detect an increased percentage of a Sm_3S_4 phase, which is formed upon SmS dissociation by the reaction [4]

$$4SmS = Sm_3S_4 + Sm \qquad (1)$$

The thermal dissociation of γ-Sm_2S_3 is accompanied with sulfur vapor evolution; as a result, the composition of the phase shifts to occur within the Sm_3S_4-Sm_2S_3 solid solution range.

The data available on SmS-base solid solution at 1800 K enables us to tentatively suggest the positions of solidus and solves lines [4]. Property-composition diagrams feature a singular point at the SmS composition. SmS is regarded as a daltonide with a two-sided solid solution (Fig. 2) [3, 23].
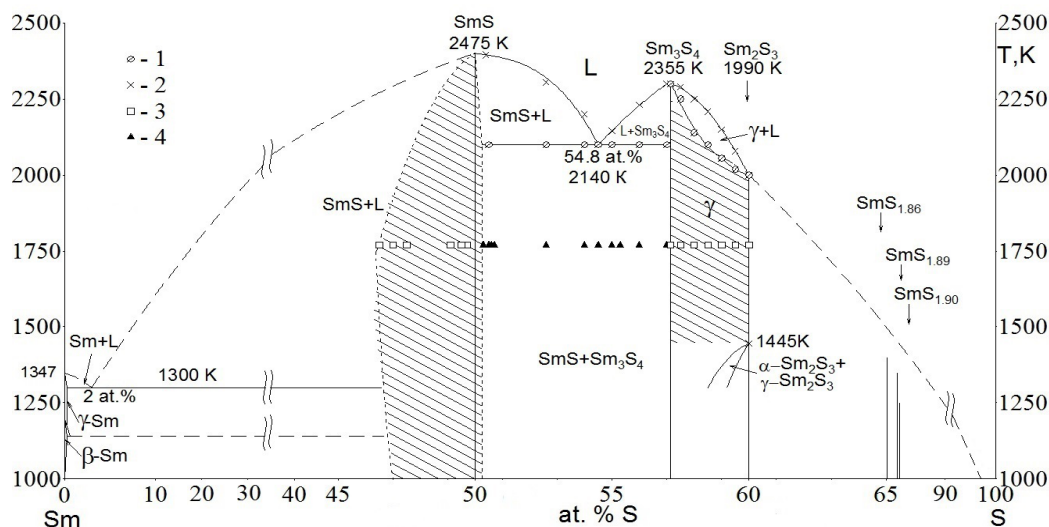

Fig. 2. Sm-S phase diagram. The state of samples as shown by VPTA: (1) incipient melting and (2) complete melting. The state of samples as shown by microstructure observation and X-ray powder diffraction measurements: (3) a single phase and (4) two phases [3, 4, 22].

A eutectic is formed between SmS and Sm_3S_4, which is distinctly identified by microstructure observation. The phase ratio in the eutectic is 0.3278 SmS + 0.6722 Sm_3S_4. The eutectic melting point in samples containing 52–56 at. % S is 2140 K as determined by VPTA (Fig. 2). Liquidus temperatures for compositions in the range 50–57.1 at. % S were determined by VPTA.

The solidus–liquidus region between Sm_3S_4 and Sm_2S_3 is cigars-shaped and classified with type 1 according to Roozeboom's classification [3].

An experimental determination of Sm-SmS eutectic coordinates meets difficulties. During synthesis, metallic samarium is deposited on ampoule walls and does not form any compact sample. The eutectic temperature as determined by DSC is (1300±10) K. The eutectic composition (2 at. % S) was calculated by empirical relationships and averaged [24].

Attempts to construct a liquidus line in the range 0–45 at. % S using high-temperature differential thermal analysis failed. Metallic samarium was sublimed from the sample in the course of heating. We have not found any data on the liquidus position in the ranges 0–45 at. % S and 60–100 at. % S. The liquidus is outlined tentatively in view of the similarity of phase equilibria in Ln-S (Ln = La-Lu; Se) systems [3, 23, 25].

Lanthanide monosulfides LnS (Ln = La-Lu) form solid solutions extending both toward an excess of rare-earth atoms and an excess of sulfur atoms [4, 18].

Solid solutions can be formed to the left and to the right of the SmS line by the following suggested scenarios.

In a samarium-rich region $Sm_{1+x}S_{1-x}\square_{2x}$, solid solutions occur due to the generation of vacant sulfur anion sites with the formation of the cationic sublattice by samarium atoms.

In a sulfur-rich region $Sm_{1-y}S_{1+y}\square_{2y}$, solid solution formation is due to the generation of samarium cation vacancies with the formation of the anionic sublattice by sulfur atoms [4, 24, 25].

The extent of samarium monosulfide solid solution is 46.5–(50.0)–50.2 at. % S [3, 4, 26-28].

Golubkov and Sergeeva [4] prepared samples of tailored compositions from the range 40–52 at. % S in sealed air-right (molybdenum or tantalum) crucibles, annealed them at 1770 K, and rapidly cooled (Table 2). Neither X-ray powder diffraction nor microstructure observation showed noticeable SmS-base solubility in the sulfur excess region.

The diagram in Fig. 2 yet shows solid solution in the range 50–50.2 at. % S. Samarium monosulfide

samples that contain Sm_3S_4 traces have decreased electrical conductivities, most likely because of the appearance of cationic vacancies in the solid solution.

When samarium atoms are in excess, $Sm_{1+x}S_{1-x}\square_{2x}$ solid solution exists in the range 46.5–50 at. % S ($x = 0$–0.035). Composition-dependent solid solution densities were calculated on the assumption that excessive samarium atoms reside either in interstices or in anionic vacancies of the SmS structure. A comparison of pycnometric densities with the calculated values implies that both types of structural alterations occur upon solid solution formation [4, 26, 27].

Electrical conductivity, thermo-EMF, and charge carrier density versus composition curves measured in the $Sm_{1+x}S_{1-x}\square_{2x}$ solution region each feature a break point at 49.7 at. % S [4, 6], 49.2 at. % S [29].

While the composition only slightly deviates from the SmS stoichiometry (49.7–50.0 at. % S, x = 0–0.003), samarium atoms prefer to occupy cationic sites, so that the electrophysical properties of samples change only insignificantly. As samarium percentage in $Sm_{1+x}S_{1-x}\square_{2x}$ solid solution increases further, the concentration of anionic vacancies increases progressively, and this inevitably results in their filling with samarium atoms [4, 29].

The delocalization of two 6s electrons of samarium atoms ($4f^26s^2$) in anionic positions, increases the electrical conductivity of solid solution samples and reduces their thermo-EMF values (Table 2).

Second phases that appear at the boundaries of SmS-base solid solution have been identified by physicochemical methods. Bluish-colored Sm_3S_4 crystals appear on polished sections as bands 1-3 μm wide embedded in between orange grains of the SmS phase. Isles of fine-grained SmS + Sm_3S_4 eutectic can also appear. In samples having compositions in the Sm + SmS solid solution region, metallic samarium appears as intergrain inclusions on the polished sections through inner portions of the sample (Table 2) [3].

The constituent elements of the Sm–S system have high partial vapor pressures. The sulfur vapor pressure versus temperature curve (590–1273 K) was fitted by a polynomial [3]:

$$\log(P_S) = 60.9106 - 24971/T + 1.081^7 \cdot 10^7/T^2 - 2.2060 \cdot 10^9/T^3 - 14.4102 \cdot \log T,$$

where P_S is saturated vapor pressure, atm; and T is temperature in degrees Kelvin.

The samarium vapor pressure is $1.28 \cdot 10^{-5}$ atm at 1000 K, $8.26 \cdot 10^{-4}$ atm at 1200 K, and 0.88 atm at 1800 K [3].

Table 2
Compositions and properties of SmS$_x$ phases [4, 26, 29]

SmS$_X$ X	Atomic % Sm	Measured density, d^{20}, g/cm^3	Unit cell parameters, A	Electrical conductivity (300 K) σ, Ω^{-1}cm^{-1}	Thermo-EMF, α μV/K	Thermal conductivity, χ*10^8 cal/(cm×s×K)	Activation energy, eV		Electron density (cm^{-3}), 10^{19}	Second phase (Sm$_3$S$_4$, Sm), mol %
							ΔE$_1$	ΔE$_2$		
1.184	45.8	5.93	5.9702 ± 2	6	240	-	0.18	0.30	0.94	46 (Sm$_3$S$_4$)
1.128	47.0	5.87	-	17	270	5.7	-	-	1.0	30
1.065	48.4	5.66	5.9712 ± 1	18	325	-	0.22	0.22	1.1	10
1.028	49.3	5.71	-	57	200	-	0.10	0.17	2.0	3
1.024	49.4	5.65	-	24	282	6.96	-	-	1.2	1
1.014	49.7	-	-	-	300	-	0.10	0.20	1.9	0.5
1.013	49.7	5.69	-	-	260	13.79	0.00	0.14	4.6	solid
1.000	50	5.69	-	36	360	15.34	0.12	0.28	9.0	solution (SS)
0.988	50.3	5.76	-	39	380	12.95	0.11	0.24	6.0	SmS
0.986	50.3	5.75	-	513	115	-	-	-	9.5	
0.980	50.5	5.75	5.9694 ± 3	500	150	10.87	-	-	7.5	
0.964	50.9	5.74	5.9693 ± 5	550	124	-	0.00	0.00	-	
0.905	52.5	-	-	870	82	-	-	-	19	
0.903	52.5	5.83	-	690	91	-	0.00	0.00	25	
0.887	53	-	-	740	96	12.2	0.00	0.00	-	
0.869	53.5	5.89	5.9706 ± 3	980	92	-	-	-	-	
0.861	53.7	5.88	5.9714 ± 3	1020	65	10.86	-	-	30	SS SmS +
0.841	54.3	5.83	5.9718 ± 4	1000	64	13.24	0.00	0.00	39	Sm
0.815	55.1	-	-	1005	65	-	-	-	20	

Heat treatment in vacuo or under argon changes the stoichiometry of a samarium sulfide phase, so that it is necessary to generate a samarium vapor or sulfur vapor atmosphere in the reactor [3, 30].

Stoichiometric Sm$_3$S$_4$ (57.14 at. % S) samples were prepared by crystallization from melt under an argon atmosphere (102 KPa) and by crystallization under a residual pressure of less than 0.1 Pa in the reactor. The Sm$_3$S$_4$ line conventionally divides the Sm–S diagram into two portions.

In order for phases containing more than 57.5 at. % S to retain their stoichiometries during heat treatment, an increased sulfur vapor pressure should be maintained in the reactor [30]. Samples of tailored compositions from the Sm$_{1+x}$S$_{1-x}$□$_{2x}$ solid solution range (x = 0–0.035) can be prepared provided that an increased samarium vapor pressure is created in the reactor (Fig. 3) [4].

The sulfur vapor pressure in the reactor with a graphite crucible is in the range of 0.3–1 atm [30] (Fig. 3). A Sm$_2$S$_3$ sample does not change its stoichiometry when heat treated in this reactor at temperatures of up to 1700 K. γ-Sm$_2$S$_3$ samples prepared in this way are typically yellow; they are transparent in the visible and IR spectral ranges; Th$_3$P$_4$ type structure; a = 0.8437 nm. Sm$_2$S$_3$ samples crystallized from melt are black; their composition

is SmS$_{1.495}$; Th$_3$P$_4$ type structure; a = 0.8440 nm.

The equilibrium sulfur vapor pressure over SmS$_{1.86}$, SmS$_{1.89}$, and SmS$_{1.90}$ polysulfides at melting temperatures is up to 30 atm (3.04 MPa) [19]. Provided that thermal dissociation is suppressed, these polysulfides should melt congruently. When polysulfide phases occur in a sealed ampoule at a temperature above 1100–1200 K, they experience thermal dissociation to form a Sm$_2$S$_3$ phase and sulfur vapor.

The reactor with a graphite crucible inside (Fig. 3) is heated to 403–443 K to provide sulfur boiling during heat treatment. This is inappropriate for an excess samarium vapor pressure to be created (the samarium melting temperature is 1345 K). One should keep in mind that metallic samarium is sublimed when heated above 1100 K, adsorbed on the walls of silica glass reactors, and then desorbed only to an insignificant degree.

The easiest-to-control conditions for treatment in samarium vapor appear in a sealed tantalum crucible containing the sample to be treated and a weighed metallic samarium sample. When the crucible is equipped with a cover and is manufactured by spot welding, a system of three-dimensional screens is mounted in the reactor to provide a local increase in samarium vapor pressure [3].
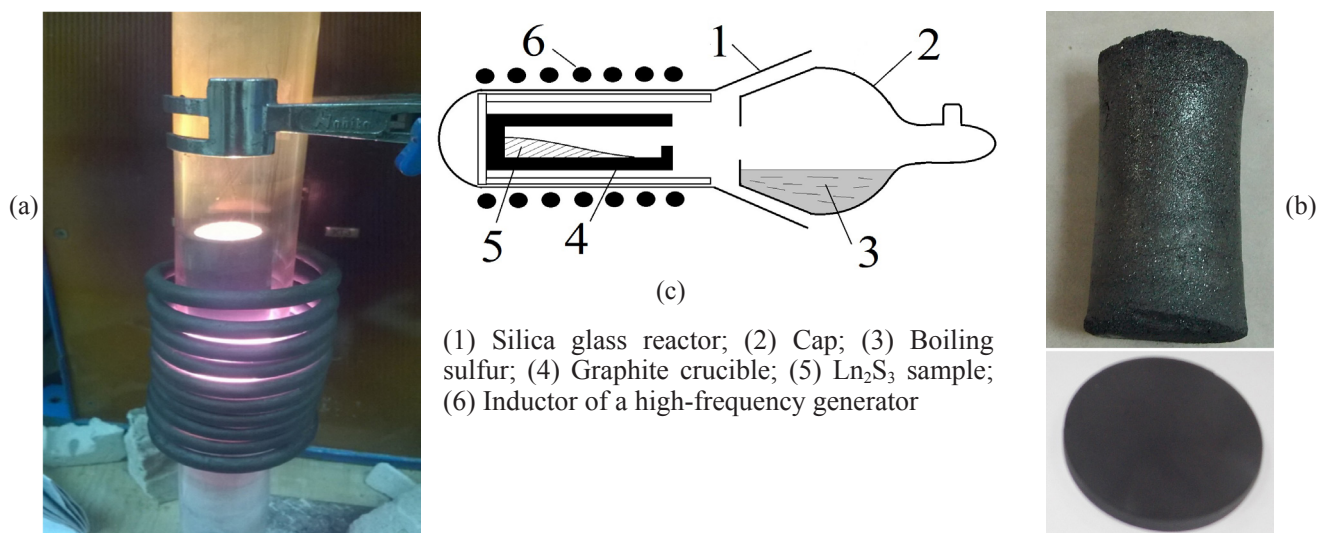
(a)

(c)

(1) Silica glass reactor; (2) Cap; (3) Boiling sulfur; (4) Graphite crucible; (5) Ln_2S_3 sample; (6) Inductor of a high-frequency generator

(b)

Fig. 3. Panel (a): annealing the batch in a tantalum crucible. Panel (b): schematics of a reactor for treating Sm_2S_3 in sulfur vapor. Panel (c): a sintered sample diameter 20 mm and a SmS disk diameter 75 mm.

Samarium monosulfide samples intended for use in flash evaporation and magnetron sputtering should have phase and chemical compositions meeting the requirements formulated as follows.

Those samples should contain at least 95 mol % SmS. Desired samarium monosulfide compositions are those within a samarium-rich region. The batch should comprise only those impurity phases that are in equilibrium with samarium monosulfide, namely Sm_3S_4 and Sm_2O_2S [31, 32]. The impurity contents in SmS as low as 1–2 mol % enhance the performance of a pressure sensor [33, 34].

In regard of the precursors and synthesis parameters, the routes to prepare samarium monosulfide may be classified in two major groups:

- inorganic syntheses;
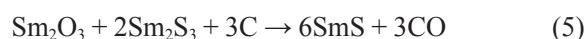
- syntheses using organometal samarium compounds.

Inorganic syntheses have the following distinguishing features, namely: high-purity precursors, staged character, high treatment temperatures (500–2000 K), special hardware, and high-cost auxiliary materials (silica glass ampoules and reactors, and tantalum or Alundum crucibles) [3, 35, 36].

Samarium monosulfide is produced in several chemical reactions:

- when samarium sulfides are reacted with metallic samarium:

$$Sm + Sm_3S_4 \rightarrow 4SmS \qquad (2)$$

$$Sm + Sm_2S_3 \rightarrow 3SmS; \qquad (3)$$

- or when samarium sesquisulfide and samarium oxysulfide are reacted with strong reducing agents.

$$3Sm_2O_2S + 3Sm_2S_3 + 4Al \rightarrow 12SmS + 2Al_2O_3 \qquad (4)$$

$$Sm_2O_3 + 2Sm_2S_3 + 3C \rightarrow 6SmS + 3CO \qquad (5)$$

The last two reactions are unsuitable for the production of samarium monosulfide. Al_2O_3 is produced in reaction (4) as a polycrystalline phase. Reaction (5) actually combines the production of metallic samarium and the reaction of the nascent metal with Sm_2S_3. These reactions occur under appreciably differing conditions. Even if the synthesis succeeds, SmS yields do not reach 60–70 mol % SmS [35, 36].

There are three commercially available products that can be used to prepare samarium monosulfide, namely metallic samarium cooled from vapor phase, Sm_2S_3, and sulfur of high-purity grade.

Reaction (3) can serve to prepare samarium monosulfide, but actual SmS yields are as low as up to 85–90 mol % [3]. Sm_2S_3 can be prepared in a flow of sulfiding gases H_2S and CS_2 according to reactions [30].

$$2Sm_2O_3 + 3CS_2 \rightarrow 2Sm_2S_3 + 3CO_2 \qquad (6)$$

$$Sm_2O_3 + 3H_2S \rightarrow Sm_2S_3 + 3H_2O \qquad (7)$$

Sm_2S_3 has a higher cost than SmS prepared from samarium and sulfur; it contains particulate carbon impurity. The grain-size composition of the powder is dominated by agglomerates having sizes of 20–50 µm, which makes difficult the occurrence of reaction (8) below to form Sm_3S_4 first and then SmS formation by reaction (2).
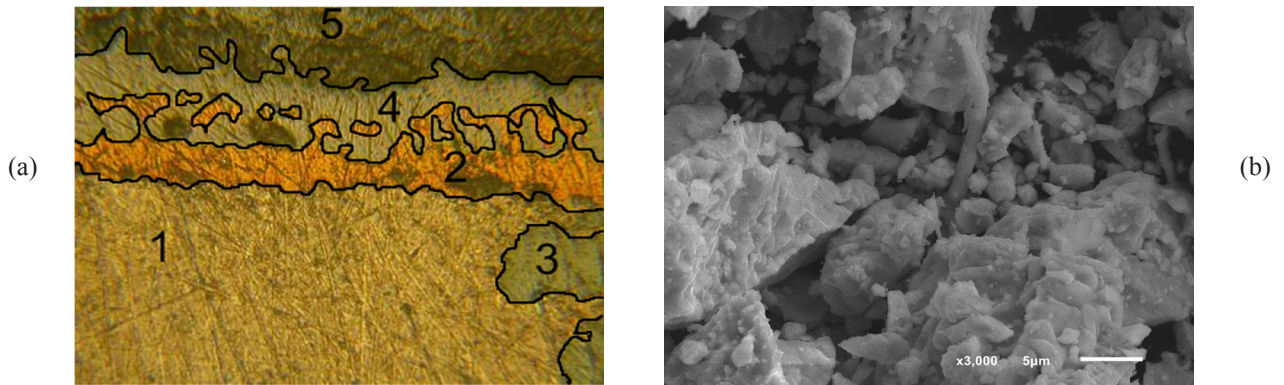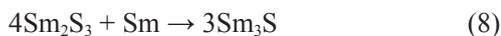
Fig. 4. Phase and grain-size compositions of a sample obtained at the ampoule synthesis stage. (a) Phase composition: (1) metallic Sm, (2) SmS, (3) Sm_3S_4, (4) α-Sm_2S_3, and (5) SmS_{2-x}. (b) Grain-size composition of the batch that contains 95 mol % SmS.

$$4Sm_2S_3 + Sm \rightarrow 3Sm_3S \qquad (8)$$

Samarium monosulfide formation from the constituent elements (metallic samarium and sulfur) involves two stages. A silica glass ampoule containing weighed samples of metallic samarium and sulfur is degassed, sealed off, and then heat-treated at 500–1200 K. The batch is sintered or alloyed inside a tantalum crucible placed in a high-frequency setup under an argon atmosphere. The reaction between metallic samarium and sulfur in a sealed ampoule involves the stage of forming layers of samarium sulfide phases in polycrystalline particles (Fig. 4) [3, 35, 36] (Fig. 4a).

In contact with metallic samarium, there is a SmS phase, next followed by Sm_3S_4, α-Sm_2S_3, and SmS_{2-x} phases. The samarium sulfide percentage in the heat-treated sample depends on the treatment temperature. At 550–700 K, a SmS_{2-x} phase is the major product. The yields of Sm_3S_4 and SmS phases increase as treatment temperature rises. The SmS

percentage in the sample after the ampoule synthesis stage is 70–90 mol %; the sample also contains Sm, Sm_3S_4, and Sm_2O_2S phases [32, 36] (Fig. 5).

The high-temperature treatment of the batch provides the occurrence of reaction (2) and the formation of tailored grain-size composition in the batch. Three temperature schedules were recognized to provide the formation of tailored phase and grain-size compositions in the batch (Fig. 5).

For reaction (2) to have the greatest completion at 1300–1600 K, an increased samarium vapor pressure should be created in the reactor. The highest SmS yields are provided by heat treatment of the batch at 1300–1800 K. At these temperatures dense grain structure starts forming [3].

In the batch annealed at 1800–2100 K, a Sm_3S_4 phase is also formed in an amount of up to 1 mol %, due to the thermal dissociation of SmS (2). Upon milling of dense-sintered samples the yield of the fraction sized 90–120 μm is up to 50%.
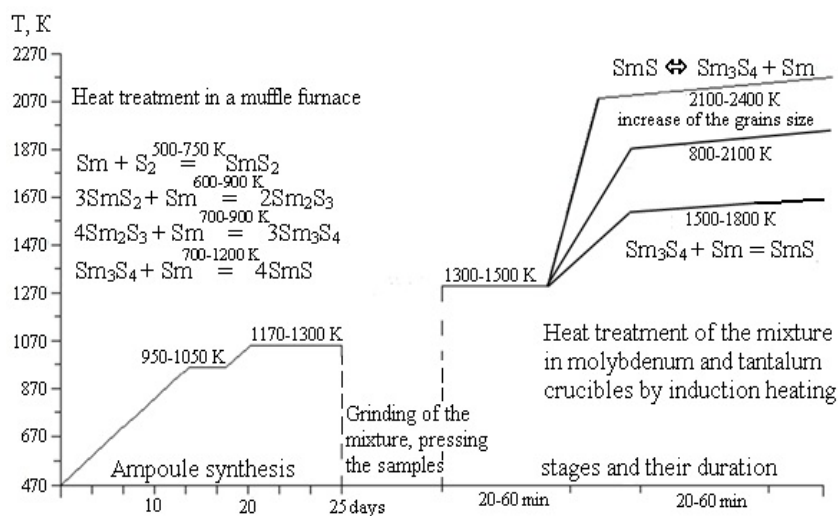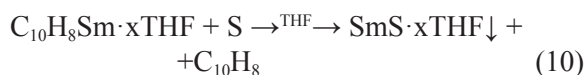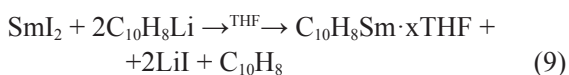

Fig. 5. Scheme of the ampoule stage and high-temperature treatment of the batch in the preparation of samarium monosulfide.

Dense-sintered samples subjected to short-term annealing at temperatures above 2100 K acquire the mechanical strength required for their use in thermoelectric generators.

The routes to prepare samarium monosulfide from organometal compounds are distinguished by the following features: low reaction temperatures (298–398 K), suitability of various classes of organic samarium compounds, available hardware, use of either sulfur or hydrogen sulfide, and the feasibility to produce samarium monosulfide in an X-ray amorphous state [37–42].

Samarium monosulfide was prepared by reacting naphthalenide with sulfur in tetrahydrofuran (THF) [37]. The preparation scheme was as follows (9, 10):

$$SmI_2 + 2C_{10}H_8Li \xrightarrow{THF} C_{10}H_8Sm \cdot xTHF + \\ +2LiI + C_{10}H_8 \qquad (9)$$

$$C_{10}H_8Sm \cdot xTHF + S \xrightarrow{THF} SmS \cdot xTHF\downarrow + \\ +C_{10}H_8 \qquad (10)$$

The final product contained SmS bonded to tetrahydrofuran.

After tetrahydrofuran was removed, SmS was obtained as an X-ray amorphous black powder.

The reaction of volatile samarium compounds with gaseous H_2S is a way to prepare an X-ray-amorphous SmS film directly on a substrate [38]:

$$[(Me_3Si)_2N]_2Sm(THF)_2 + H_2S \rightarrow SmS(THF)_x + \\ +2(Me_3Si)_2NH \qquad (11)$$
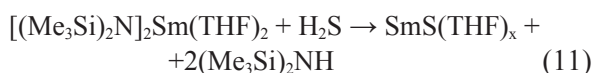
The thus-prepared film is then thermally annealed in stages to be converted to a polycrystalline state [38].

In [40] the chemical synthesis of the Smx-SyOz compounds is performed by thermolysis of dithiocarbamate precursors, followed by the drop casting deposition of the synthesized material, and by the thermal treatment at different temperatures (250 °C, 500 °C and 900 °C) and atmospheric conditions (nitrogen and air). The temperature of 900 °C and the nitrogen atmosphere represent the optimal treatment conditions, among the process parameters, to obtain a single phase of Sm_2SO_2.

At the work [41, 42] samarium dithiocarbamates were obtained in form dte$_3$Smbipy, dte$_3$Smphen, dte$_3$Sm. Substances were ~~saluted~~ in pyridine and thermally decomposed on the pyroceramics support at 450–570 K. Polycrystalline films SmS a = 5.6 –5.7 Å containing impurities were obtained.
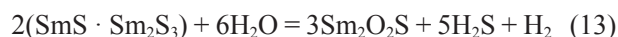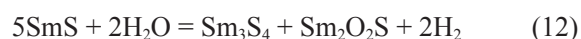
The chemical properties of SmS are determined by the electronic structure of samarium and its oxidation state 2+ in $Sm^{2+}S^{2-}$. In the settings of an air atmosphere where the oxygen partial vapor pressure $p(O_2)$ = 0.21 atm, stable oxygenated and halide compounds are those where samarium has the oxidation state +3, for example Sm_2O_3, SmF_3, $SmCl_3$, $Sm_2(SO_4)_3$, Sm_2O_2S, Sm_2S_3 and others [3, 22, 32, 43].

Reactions of SmS with water or acids involve concurrent ion-exchange and redox reactions [31, 43].

Polycrystalline SmS powders are stable under air. The phase composition of a SmS powder (the fraction sized 60–100 μm) after 30 years of exposure to dry air changed only insignificantly, so that the percentage of the Sm_2O_2S increased by 3–5 mol % [31].

Samarium monosulfide should be regarded as a salt of a weak hydroxide $Sm(OH)_2$ (an unstable compound) and a weak acid H_2S; such compounds are completely hydrolysable in aqueous media. A polycrystalline SmS powder (fraction sized 90–120 μm) experiences only surface hydrolysis when exposed to H_2O for 10 h. The degree of hydrolysis does not increase appreciably after the powder is exposed to boiling water for 1 h. In the bulk of polycrystalline grains, the phase composition remains unchanged.

The products of reaction (12) between SmS and H_2O in the course of thermohydrolysis are detected in the vapor phase when reaction zone temperatures are 600–650 K [3, 31, 44]. The presence of H_2 in the vapor phase was proven chromatographically. The hydrolysis yields a Sm_3S_4 phase, which subsequently also reacts with H_2O according to reaction (13) below.

$$5SmS + 2H_2O = Sm_3S_4 + Sm_2O_2S + 2H_2 \qquad (12)$$

$$2(SmS \cdot Sm_2S_3) + 6H_2O = 3Sm_2O_2S + 5H_2S + H_2 \quad (13)$$

The chemism of SmS oxidation is in many traits similar to the hydrolysis chemism. A SmS powder after the ampoule synthesis stage having particle sizes of 3–15 μm, oxidizes in flowing air starting at 520–570 K. Sintered technical ceramics withstand oxidation when exposed to temperatures up to 650 K for 1 h. The oxidation of SmS powder is accompanied with an increase in Sm_3S_4 percentage formed by reactions (13) and (14) (Fig. 6) [45].

$$5SmS + O_2 = Sm_2O_2S + Sm_3S_4 \qquad (14)$$

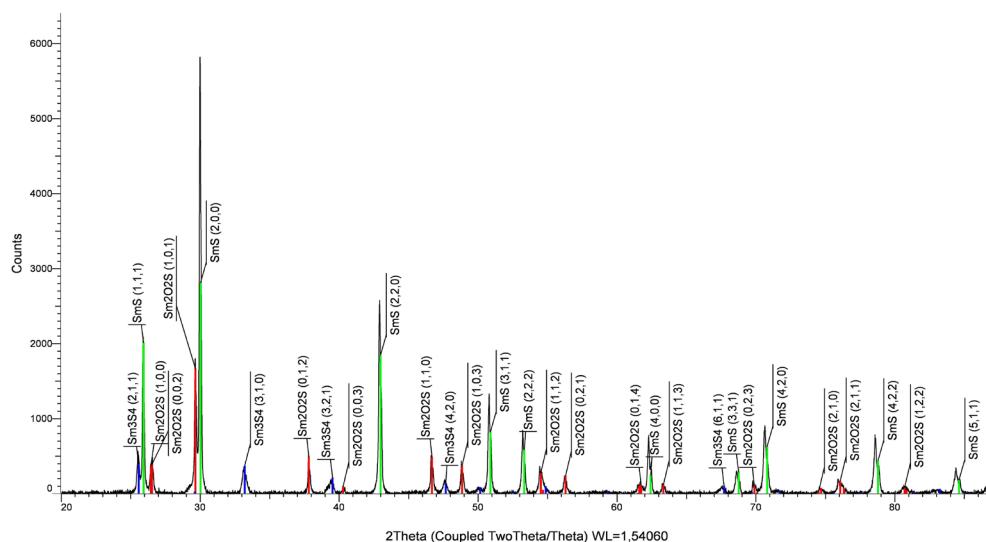$$Sm_3S_4 + 8O_2 = Sm_2O_2S + 5SO_2 \qquad (15)$$
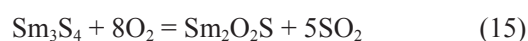
Fig. 6. X-ray diffraction pattern for a SmS ceramic sample oxidized in the course of heat treatment. Phase contents in the sample: 53.34 mol % SmS, 9.84% Sm_3S_4, and 36.82% Sm_2O_2S.

The reaction of SmS with an acid (HHal, HNO_3, or H_2SO_4) involves concurrent ion-exchange and redox reactions, described by reaction (16) below.

$$2SmS + 2HCl + 2H_2O = 2Sm(OH)_2Cl + H_2S + H_2 \quad (16)$$

Samarium monosulfide, a stable compound in polycrystalline state, has properties similar to isostructural compounds CaS, SrS, and BaS (rCa^{2+}(CN=6) = 1.140 Å, rSr^{2+}(CN=6) = 1.320 Å, rBa^{2+}(CN=6) = 1.490 Å, and rSm^{2+}(CN=6) = 1.360 Å) [30, 43].

Now there are two main routes to prepare samarium monosulfide films, namely flash evaporation and magnetron sputtering [3, 33, 46].

In flash evaporation, the precursor is a SmS fraction with grain sizes of 90–120 μm. Evaporation is performed in a high vacuum (0.001 Pa). A SmS powder is conveyed by the Archimedes screw from the hopper to a tungsten heater maintained at 2670 K. Optimal is the "blue torch" mode where a fallen SmS grain is sublimed immediately. Serial SmS sensors manufactured by flash evaporation have pressure sensitivity coefficients of 30–50 [33, 34]. In $Sm_{1-x}Eu_xS$ solid solution the magnitude of effects is increased [47, 48].

A SmS disk to be used in magnetron sputtering should meet certain requirements as to mechanical strength. A ceramic disk 75 mm in diameter was manufactured by compacting SmS powder and then sintered at 1500–1600 K. Magnetron sputtering makes it possible to form films of tailored thickness with tailored sensor parameters. Thin SmS films in addition manifest the photoelectric effect, and thereby create additional opportunities for use of samarium monosulfide.

The materials that are in contact with SmS bulk samples or films, should not chemically react with those bulk samples or films. Chemical compounds or noticeable solid solutions formed in the contact layer change the resistance of the circuit and, with time, can interfere with the readings of sensor [33, 34].

Nickel is the major contact material used; metallic titanium, aluminum, and gold can also be used. No increase in ohmic resistance was detected during the performance of many hundreds of SmS sensors equipped with a nickel contact. Aluminum is of interest in this context for the fact that subsequent surface oxidation to Al_2O_3 provides chemical protection to the contact.

It is undesirable to use conventional electroengineering materials, such as copper and silver. There is a tie-line between Cu and SmS phases in Cu-Sm-S and Ag-Sm-S ternary systems.

$Cu_{2-x}S$ and $Ag_{2-x}S$ phases are thermally stable, which makes their local formation possible. Copper and, especially, silver react with sulfur even at 300 K. When metallic silver or copper is in contact with a SmS phase for a long time $Ag_{2-x}S$ or $Cu_{2-x}S$ isles are formed; the film composition shifts to appear in the samarium-rich solid solution [49, 50].

Acknowledgements

References

[1]. I. Groshev, I. Poluhin, Komponenty i tehnologii [Components and technologies] 8 (2014) 126–133 (in Russian).

[2]. V.V. Kaminskiy, N.N. Stepenov, N.M. Volodin, Yu.N. Mishin, raketnaja tehnika i kosmonavtika [Astronautics and missilery] 17 (1) (2013) 11–16. (in Russian).

[3]. O.V. Andreev, L.N. Monina, V.O. Andreev, A.V. Elyishev, O.Yu. Mitroshin. Phase equilibria, synthesis, phase structure in the 3d-, 4f-elements sulphides systems. Textbook. Tyumen: Tyumen State University Publishing. 2014. 512 p. (in Rissian).

[4]. A.V. Golubkov, V.M. Sergeeva, Russian Journal of General Chemistry 26 (6) (1981) 645 – 653.

[5]. V.V. Kaminskiy, T. Kuzuya, S.Hirai, C.M. Soloviev, Physics of the Solid State 54 (7) (2012) 1269–1271.

[6]. V.V. Kaminskiy, N.V. Sharenkova, L.V. Vasil'yev, S.M. Solov'yev, Physics of the Solid State 47 (2) (2005) 217–219.

[7]. V.V. Kaminskiy, N.N. Stepanov, A.A. Molodykh, Physics of the Solid State 52 (7) (2010) 1269–1270.

[8]. V.V. Kaminskiy, V.A. Sidorov, N.N. Stepanov, M.M. Kazanin, A.A. Molodykh, S.M. Solov'yev, Physics of the Solid State 55 (2) (2013) 257–259.

[9]. I.N. Barinov. Components and technologies 5 (2009) 12–15.

[10]. Y.I. Sucharev, T.I. Prolubnikova, I.I. Lebedeva. Eurasian Chemico-Technological Journal 14 (1) (2012) 61–72.

[11]. O. Prikhodko, N. Almasov, N. Korobova, Eurasian Chemico-Technological Journal 12 (3) (2010) 279 – 283.

[12]. V.M. Egorov, V.V. Kaminskiy, M.M. Kazanin, S.M. Solov'yev, A.V. Golubkov, Technical Physics Letters 41 (8) (2015) 50–54.

[13]. V.V. Kaminskiy, S.M. Solov'yev, A.V. Golubkov, Technical Physics Letters 28 (6) (2002) 29–54.

[14]. V.V. Kaminskikh, M.M. Kazanin, A.N. Klishin, S.M. Solov'yev, A.V. Golubkov, Technical Physics 81 (6) (2011) 150–152.

[15]. V.V. Kaminskiy, S.M. Solov'yev, Technical Physics Letters 31 (14) (2005) 45–49.

[16]. V.M. Egorov, V.V. Kaminskiy, Physics of the Solid State 51 (8) (2009) 1521–1522.

[17]. D.V. Zhuravskiy, G.P. Laskin, K.V. Misibk, S.Yu. Udovichenko. Tyumen state university herald 7 (2013) 98–103 (in Russian).

[18]. E.I. Yarembash and A.A. Eliseev. Rare-earth metal chalcogenides. Nauka. Moskow. 1975. 260 p. (in Russian).

[19]. I.G. Vasileva, Russian Journal of Physical Chemistry A. 80 (11) (2006) 1842 – 1847.

[20]. G.M. Kuz'micheva, O.V. Andreev, N.N. Parshukov, O.N. Reshetnikova, Russian Journal of Inorganic Chemistry 42 (11) (1997)1790–1792.

[21]. N.V. Podberezskaya, N.V. Pervuhina, I.G. Vasileva, S.A. Magarill, S.V. Borisov, Journal of Structural Chemistry 40 (3) (1999) 520–529.

[22]. I.G. Vasileva, Ya.I. Gibner, L.N. Kurochkina, Inorganic Materials 19 (3) (1983) 360–362.

[23]. O.V. Andreev, G.M. Kuzmicheva, N.N. Parshukov, S.S. Sikerin, Russian Journal of Inorganic Chemistry 44 (6) (1999)1024–1027.

[24]. A.A. Ganeev, A.R. Halikov, R.R. Karibov USATU Herald 11 (2) (2008) 116–122 (in Russian).

[25]. O.V. Andreev, V.B. Kharitonstsev, A.A. Polkovnikov, A.V. Elyshev, P.O. Andreev, Journal of Solid State Chemistry 7 (2015) 186–190.

[26]. V.M. Egorov, Fei Wang, V.V. Kaminskiy, Shinji Hirai, N.V. Sharenkova, Physics of the Solid State. 54 (1) (2012) 46–49.

[27]. K. Imura, K. Matsubayashi, H.S. Suzuki, K. Deguchi, N.K. Sato. Journal of Physics: Conference Series 121 (2008). P. 032014.

[28]. K. Matsubayashi, K. Imura, H.S. Suzuki, T. Mizuno, S. Kimura, T. Nishioka, K. Kodama, N.K. Sato, J. Phys. Soc. Jpn. 76 (6) (2007) 064601-1 – 064601-6.

[29]. A.V. Golubkov, M.M. Kazanin, V.V. Kaminskii, V.V. Sokolov, S.M. Solov'ev, L.N. Trushinikova. Inorganic Materials 39 (12) (2003) 1251–1256.

[30]. V.G. Bamburov, O.V. Andreev, Russian Journal of Inorganic Chemistry 47 (4) (2002) 676–683.

[31]. P.V. Miodushevsky, P.O. Andreev, A.S. Vjsokih. Omsk University herald 4 (2011) 122–126 (in Russian).

[32]. O.V. Andreev, A.S. Vysokikh, V.G. Vaulin. Russian Journal of Inorganic Chemistry 53 (8) (2008) 1414–1418.

[33]. N.M. Volodin, Yu.N. Mishin, V.V. Kaminskiy, Yu.V. Zakharov. Lavochkin Association 2 (2012) 33–37 (in Russian).

[34]. N.M. Volodin, Yu.N. Mishin, V.V. Kaminskiy, Lavochkin Association 5 (2011) 51–55 (in Russian).

[35]. O.V. Andreev, N.N. Parshukov, V.M. Andreeva, Russian Journal of Inorganic Chemistry 39 (1) (1994) 6–9.

[36]. O.V. Andreev, O.A. Sadovskaya, E.Yu. Shabalina, Russian Journal of Inorganic Chemistry 35 (3) (1990) 11–16.

[37]. O.V. Andreev, M.N. Bochkarev, N.M. Volodin, T.V. Nekrasova, A.V. Protchenko, Organometallic chemistry 2 (1993) 1361–1362.

[38]. O.V. Andreev, M.N. Bochkarev, T.V. Nekrasova, A.V. Protchenko, Russian Chemical Bulletin 44 (2) (1995) 233–235.

[39]. Michelle D. Regulacio, Neil Tomson, Sarah L. Stoll, Chem. Mater. 17 (2005) 3114–3121.

[40]. M.A. Signore, A. Taurino, M. Catalano, E. Bellini, G. DiGirolamo, A.M. Laera, F. Quaranta, L. Vasanelli, P. Siciliano, Thin Solid Films 556 (2014) 241–246.

[41]. M. Volodin, L.V. Zavyalova, A.I. Kirillov, S.V.

Svechnikov, I.V. Prokopenko, A.V. Khanova, Semiconductor Physics, Quantum Electronics Optoelectronics 2 (2) (1999) 78–83.

[42]. G.A. Domrachev, L.V. Zav'yalova, G.S. Svechnikov, O.N. Suvorova, A.V. Khanova, E.A. Shchupak, L.A. Yarosh. Russian Journal of General Chemistry 73 (4) (2003) 593–599.

[43]. O.V. Andreev, V.G. Bamburov, L.N. Monina, I.A. Razumkova, A.V. Ruseykina, O.Yu. Mitroshin, V.O. Andreev. Phase equilibria in the sulfide systems of the 3d-, 4f- elements. Ekaterrinburg, 2015. 309 p. (In Russian).

[44]. A.S. Vysokikh, O.V. Andreev, L.A. Golovina. Tyumen state university herald 3 (2007) 124–129 (in Russian).

[45]. O.V. Andreev, A.S. Vysokikh, I.P. Leven. Physical chemistry of high-tech materials. Taymen. 2007. 88 p. (in Russian).

[46]. V. V. Kaminskii, M.M. Kazanin, Technical Physics Letters 34 (4) (2008) 361–362.

[47]. A.V. Golubkov, V.A. Didik, V.V. Kaminskii, E.A. Skoryatina, V.P. Usacheva, N.V. Sharenkova. Physics of the Solid State 47 (7) (2005) 1233–1235.

[48]. V.V. Kaminskii, M.M. Kazanin, L.N. Golubkov, Technical Physics 82 (6) (2012) 142–144.

[49]. O.V. Andreev, Russian Journal of Inorganic Chemistry 34 (6) (1989) 1603–1606.

[50]. O.V. Andreev, Russian Journal of Inorganic Chemistry 34 (2) (1989) 482–486.